2,2'-Bipyrimidine (bipym)-bridged Dinuclear Complexes. Part 1. Preparation, Crystal Structure, and Magnetic Properties of $[Ni_2(H_2O)_8(bipym)][NO_3]_4$ and $[Ni_2(H_2O)_8(bipym)][SO_4]_2 \cdot 2H_2O$†

Giovanni De Munno,[a] Miguel Julve,*[,b] Francesc Lloret[b] and Alain Derory[c]

[a] *Dipartimento di Chimica, Università degli Studi della Calabria, 87030 Arcavacata di Rende (Cosenza), Italy*

[b] *Departament de Química Inorgànica, Facultat de Química de la Universitat de València, Dr. Moliner 50, 46100 Burjassot (València), Spain*

[c] *IPCSM, Groupe de Chimie des Matériaux Inorganiques, UM-380046-EHICS, 1 Rue Blaise Pascal, Strasbourg, France*

Two new dinuclear nickel(II) complexes of formula $[Ni_2(H_2O)_8(bipym)][NO_3]_4$ **1** and $[Ni_2(H_2O)_8(bipym)][SO_4]_2 \cdot 2H_2O$ **2** (bipym = 2,2'-bipyrimidine) have been synthesised and their crystal structures determined by X-ray crystallographic methods. Crystals of **1** and **2** are monoclinic, space group $P2_1/n$ with $a = 10.020(2)$, $b = 10.521(2)$, $c = 11.019(2)$ Å, $\beta = 90.27(1)°$ and $Z = 2$ for **1** and space group $P2_1/c$ with $a = 8.094(2)$, $b = 11.550(3)$, $c = 11.719(2)$ Å, $\beta = 91.85(1)°$ and $Z = 2$ for **2**. Both structures consist of centrosymmetrical dinuclear cations $[Ni_2(H_2O)_8(bipym)]^{4+}$ with nitrate counter ions for **1** and water of crystallization and sulfate counter ions for **2**. Each nickel atom is six-co-ordinated in a slightly distorted octahedral NiN_2O_4 chromophore: the average Ni^{II}–N distance is 2.094 Å in **1** and 2.115(2) Å in **2**, whereas the mean Ni^{II}–O distance is 2.094(3) Å in **1** and 2.056(2) Å in **2**. The bipyrimidine group joins two adjacent nickel atoms acting as a bis(bidentate) ligand. The C–C bond between the pyrimidine rings of bipym is perpendicular to the Ni ··· Ni vector giving two five-membered chelate rings. The intramolecular Ni ··· Ni separation is 5.569(1) Å for **1** and 5.660(1) Å for **2**. Intramolecular antiferromagnetic spin-exchange coupling between the two nickel(II) ions is observed in both complexes with $J = -14$ and -12 cm^{-1} for **1** and **2**, respectively (J is the intradimer exchange parameter in the isotropic Hamiltonian $\hat{H} = -J\hat{S}_A \cdot \hat{S}_B$). The efficiency of bipym to transmit electronic effects is compared to that of related bis(chelating) ligands such as oxalate and oxamidate in the parent oxalate- and oxamidate-bridged nickel(II) complexes.

2,2'-Bipyrimidine (hereafter bipym) can act as a chelating or bis(chelating) ligand toward transition-metal ions to yield mono- and poly-nuclear complexes, respectively.[1–6] Considerable attention has been paid to this kind of ligand and analogues containing π-electron delocalization because they can be seen as potential electron propagating components in (*i*) electron-transfer reactions between metal centres, (*ii*) magnetic exchange interactions in polynuclear systems, (*iii*) model systems for biological studies and (*iv*) the design of light-capturing antennas *via* charge-transfer transitions.[7] Our current research work concerns the second field and in this respect we have undertaken a systematic study dealing with the synthesis, structural characterization and magnetic properties of polynuclear complexes between bipym and first-row transition-metal ions. As a first step, we restricted ourselves to the Cu^{II}–bipym system. The presence of only one unpaired electron per metal centre, the lack of orbital contribution to the magnetic moment and the rich stereochemistry of Cu^{II} ensuing from the plasticity of its co-ordination sphere are the main reasons for this choice. A large antiferromagnetic contribution (singlet–triplet energy gap from -236 to -191 cm^{-1}) was found in the series $[Cu_2(bipym)X_4]$ (X = Cl, Br or NO_3)[5b,f] which is due to the large σ-in plane overlap of the $d_{x^2-y^2}$ magnetic metal orbitals through the bipym bridge. More recently, it was shown how the Cu^{II}:bipym molar ratio can be used as a suitable tool to prepare mono-, di-nuclear and one-dimensional compounds by reaction of copper(II) perchlorate and bipym in aqueous solution.[8] Our last attempt dealt with the design of one-, two- and three-dimensional networks {compounds of formula $[Cu(bipym)(NCS)_2]$, $[Cu_2(bipym)(NCO)_4]$ and $[Cu_2(bipym)(NCS)_4]$, respectively} playing on both the Cu^{II}:bipym molar ratio and the nature of the counter ion X.[9]

Structural data for bipym-containing complexes of first-row transition-metal ions other than Cu^{II} are scarce. At this respect, the structures of only three complexes, one mononuclear $[Co(bipym)_2Cl_2]$,[6h] and two dinuclear $[Co_2(hfacac)_2(bipym)]$[5c] and $[Fe_2(bpm)_2(bipym)(NCS)_4]$,[5e] {hfacac = hexafluoroacetylacetonate and bpm = bromoazepam[7-bromo-1,3-dihydro-5-(2-pyridyl)-2*H*-1,4-benzodiazepin-2-one]}, are known. Variable-temperature magnetic data for these dinuclear species as well as of related bipym-bridged complexes of Mn^{II} and Ni^{II} revealed weak coupling constants.

In the present work we report on the preparation, structural determination and spectroscopic and magnetic characterization of two new bipym-bridged nickel(II) complexes of formula $[Ni_2(H_2O)_8(bipym)][NO_3]_4$ **1** and $[Ni_2(H_2O)_8(bipym)][SO_4]_2 \cdot 2H_2O$ **2**.

Experimental

Materials.—2,2'-Bipyrimidine, nickel(II) nitrate hexahydrate

† *Supplementary data available:* see Instructions for Authors, *J. Chem. Soc., Dalton Trans.*, 1993, Issue 1, pp. xxiii–xxviii.

Non-SI unit employed: emu = SI × $10^6/4\pi$. B.M. ≈ 9.27×10^{-24} $J\,T^{-1}$.

and nickel(II) sulfate heptahydrate were purchased from commercial sources and used as received. Elemental analyses (C, H, N) were conducted by the Microanalytical Service of the Universidad Autónoma de Madrid (Spain).

Preparation of $[Ni_2(H_2O)_8(bipym)][NO_3]_4$ **1** *and* $[Ni_2(H_2O)_8(bipym)][SO_4]_2 \cdot 2H_2O$ **2**.—Both complexes were synthesised by mixing an aqueous solution of the corresponding nickel(II) salt (1 mmol, 50 cm^3) and an ethanolic solution of bipym (0.5 mmol, 10 cm^3). Polyhedral pale blue-green crystals of **2** separated after a few days upon slow evaporation at room temperature. Complex **1** is very soluble in water and chunky pale blue crystals were obtained when nearly all the solution was evaporated. Crystals of it suitable for X-ray analysis were obtained by cutting some of these (Found: C, 13.95; H, 3.20; N, 16.20. Calc. for $C_8H_{22}N_8Ni_2O_{20}$ **1**: C, 14.40; H, 3.30; N, 16.80. Found: C, 14.60; H, 4.10; N, 8.40. Calc. for $C_8H_{26}N_4Ni_2O_{18}S_2$ **2**: C, 14.85; H, 4.05; N, 8.65%).

Physical Techniques.—The infrared spectra were taken on a Perkin Elmer 1750 spectrophotometer as KBr pellets in the 4000–300 cm^{-1} region and the electronic spectra with a Perkin Elmer Lambda-9 UV/VIS spectrophotometer as Nujol mulls on filter-paper. Variable-temperature magnetic susceptibility measurements were carried out in the range 4.2–300 K with a fully automatized AZTEC DSM5 pendulum-type susceptometer equipped with a TBT continuous-flow cryostat and a Brüker BE15 electromagnet, operating at 1.8 T. The apparatus was calibrated with $Hg[Co(NCS)_4]$. Corrections for the diamagnetism of complexes **1** and **2** were estimated from Pascal's constants as -308×10^{-6} and -339×10^{-6} emu mol^{-1}, respectively. Experimental susceptibilities were also corrected for the temperature-independent paramagnetism (-100×10^{-6} emu per Ni^{II}).

Crystal Structure Determination and Refinement.—Diffraction data for complexes **1** and **2** were collected at 298 K with a Siemens R3m/V automatic four-circle diffractometer using graphite-monochromated Mo-Kα radiation (λ = 0.710 69 Å). Crystal parameters and pertinent refinement results are summarized in Table 1. The unit-cell parameters were determined from least-squares refinement of the setting angles of 25 reflections in the range 2θ 14–30°. A total of 3136 (**1**) and 2845 (**2**) reflections were collected by the variable-speed ω–2θ scan method in the range 2θ 3–55° with index ranges $0 \leqslant h \leqslant 13, 0 \leqslant k \leqslant 13, -14 \leqslant l \leqslant 14$ for **1** and $0 \leqslant h \leqslant 10$, $0 \leqslant k \leqslant 15, -15 \leqslant l \leqslant 15$ for **2**; 2688 (**1**) and 2533 (**2**) of them were unique, and of these 2249 (**1**) and 2062 (**2**) were assumed as observed [$I > 3\sigma(I)$] and used for the refinement of the structures. Examination of three standard reflections, monitored after every 100, showed no sign of crystal deterioration. The usual corrections for Lorentz and polarization effects were carried out. ψ-Scan absorption correction [10] was also applied to the intensity data. The maximum and minimum transmission factors were 0.401 and 0.361 for **1** and 0.637 and 0.580 for **2**.

The structures were solved by Patterson methods with the SHELXTL PLUS program [11] followed by successive Fourier syntheses and full-matrix least-squares refinements based on $|F_o|$. All non-hydrogen atoms were refined anisotropically. The hydrogen atoms of the water molecules were located on a ΔF map and refined with constraints. The hydrogen atoms of bipym were set in calculated positions and refined as riding atoms. A common fixed isotropic thermal parameter was assigned to all hydrogen atoms. The final full-matrix least-squares refinement, minimizing the function $\Sigma w(||F_o| - |F_c||)^2$ with $w = 1/[\sigma^2(F_o) + q(F_o)^2]$ and $q = 0.002\,000$ (**1**) and 0.000 347 (**2**) [with $\sigma^2(F_o)$ from counting statistics], converged at R and R' indices of 0.0454 and 0.0560 for **1** and 0.0273 and 0.0295 for **2**. The number of reflections/number of variable parameters was 11.5 and 11.2 for **1** and **2**, respectively. In the final difference map the residual maxima and minima were 1.05 and -0.68 e $Å^{-3}$ for **1** and 0.44 and -0.49 e $Å^{-3}$ for **2**. The largest and mean Δ/σ are 0.140 and 0.006 for **1** and 0.313 and 0.014 for **2**. Atomic scattering factors and corrections for anomalous dispersion for Ni and S atoms were taken from ref. 12. All calculations were carried out on a MICRO-VAX II computer, using the SHELXTL and PARST [13] program package. The graphical manipulations were performed using the XP utility of the SHELXTL PLUS system. The final atomic coordinates for non-hydrogen atoms and selected interatomic bond distances and angles around nickel(II) together with the hydrogen bonding for compounds **1** and **2** are given in Tables 2–5.

Additional material available from the Cambridge Crystallographic Data Centre comprises H-atom coordinates, thermal parameters and remaining bond lengths and angles.

Results and Discussion

Structures of Complexes **1** *and* **2**.—The structures of complexes **1** and **2** are made up of μ-(2,2′-bipyrimidine-*N*,*N*′,*N*″,*N*‴)-bis[tetraaquanickel(II)] dinuclear cations with a crystallographically imposed inversion centre located halfway between the halves of the bipym molecule, and unco-ordinated nitrate (**1**) and sulfate (**2**) anions. Two water molecules of crystallization are also present in **2**. The molecular geometry and the atom labelling scheme for the cation of **1** (identical labelling was adopted for **2**) is illustrated by Fig. 1. The nitrate and sulfate counter ions contribute to the packing by forming an extensive network of hydrogen bonds involving oxygen atoms and co-ordinated and unco-ordinated water molecules

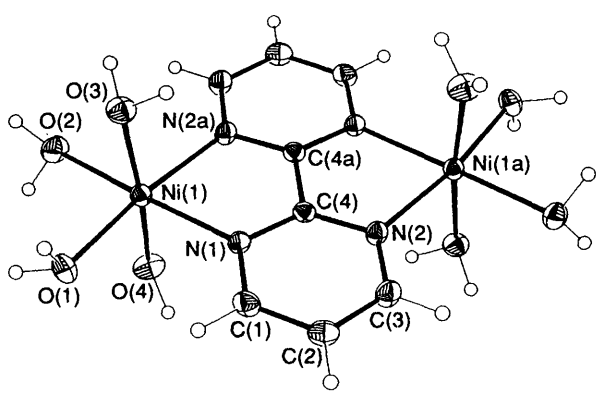

Fig. 1 A perspective view of the cationic unit $[Ni_2(H_2O)_8(bipym)]^{4+}$ of complex **1** showing the atom labelling. Thermal ellipsoids are drawn at the 30% probability level

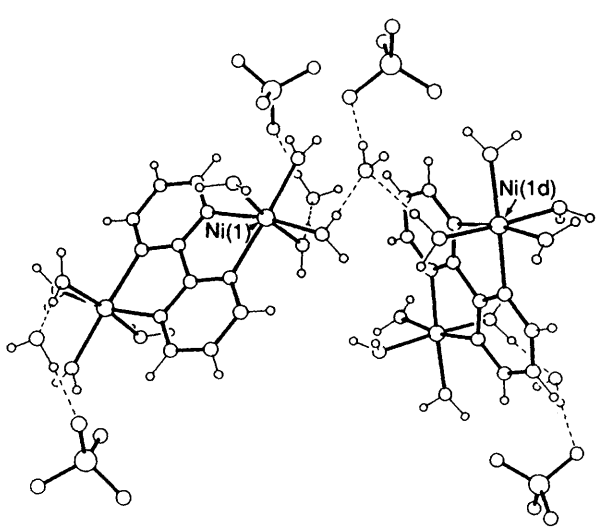

Fig. 2 Hydrogen-bonding interactions (dashed lines) in complex **2**

Table 1 Crystallographic data for $[Ni_2(H_2O)_8(bipym)][NO_3]_4$ **1** and $[Ni_2(H_2O)_8(bipym)][SO_4]_2 \cdot 2H_2O$ **2**

Compound	**1**	**2**
Formula	$C_8H_{22}N_8Ni_2O_{20}$	$C_8H_{26}N_4Ni_2O_{18}S_2$
M	667.8	647.9
Crystal system	Monoclinic	Monoclinic
Space group	$P2_1/n$	$P2_1/c$
a/Å	10.020(2)	8.094(2)
b/Å	10.521(2)	11.550(3)
c/Å	11.019(2)	11.719(2)
β/°	90.27(1)	91.85(1)
U/Å^3	1161.6(4)	1095.0(4)
Z	2	2
D_c/kg m^{-3}	1.909	1.965
$F(000)$	684	668
Crystal size/mm	0.32 × 0.39 × 0.51	0.11 × 0.18 × 0.25
μ(Mo-Kα)/cm^{-1}	17.3	20.0
No. of refined parameters, N_p	196	184
$R[=\Sigma(\|\|F_o\| - \|F_c\|\|)/\Sigma\|F_o\|]$	0.0454	0.0273
$R'\{=[\Sigma(\|\|F_o\| - \|F_c\|\|)^2/\Sigma w\|F_o\|^2]^{\frac{1}{2}}\}$	0.0560	0.0295
s*	1.52	1.31

* Goodness of fit $= [\Sigma w(\|\|F_o\| - \|F_c\|\|)^2/(N_o - N_p)]^{\frac{1}{2}}$.

Table 2 Final atomic coordinates for complex **1** with estimated standard deviations (e.s.d.s) in parentheses

Atom	X/a	Y/b	Z/c
Ni(1)	0.1902(1)	0.1944(1)	0.0109(1)
O(1)	0.1704(3)	0.3879(3)	0.0086(2)
O(2)	0.3958(3)	0.2057(3)	0.0103(3)
O(3)	0.1980(3)	0.1987(2)	0.1962(2)
O(4)	0.2036(3)	0.1947(3)	−0.1744(3)
O(5)	0.4790(3)	0.3709(3)	−0.1690(3)
O(6)	0.3790(3)	0.5306(3)	−0.0890(3)
O(7)	0.5507(4)	0.5600(3)	−0.2014(4)
O(8)	0.3883(4)	0.0265(4)	0.2865(4)
O(9)	0.5593(4)	0.0866(5)	0.2771(4)
O(10)	0.5635(6)	0.1042(6)	0.2057(5)
N(1)	−0.0167(3)	0.1688(2)	0.0029(3)
N(2)	−0.1780(2)	0.0046(3)	−0.0115(2)
N(3)	0.4689(3)	0.4884(3)	−0.1544(3)
N(4)	0.5090(4)	0.0173(4)	0.2555(3)
C(1)	−0.1145(3)	0.2562(3)	−0.0032(3)
C(2)	−0.2455(4)	0.2202(3)	−0.0142(3)
C(3)	−0.2748(3)	0.0922(3)	−0.0185(3)
C(4)	−0.0539(3)	0.0479(3)	−0.0024(3)

Table 3 Final atomic coordinates for complex **2** with e.s.d.s in parentheses

Atom	X/a	Y/b	Z/c
Ni(1)	0.1812(1)	0.1041(1)	0.1833(1)
S(1)	0.7290(1)	0.2844(1)	−0.0199(1)
O(1)	0.4149(2)	0.1764(2)	0.2103(2)
O(2)	0.1177(3)	0.1389(2)	0.3467(2)
O(3)	0.1078(2)	0.2683(2)	0.1433(2)
O(4)	0.2722(2)	−0.0549(2)	0.2365(2)
O(5)	0.8416(2)	0.2297(2)	−0.1002(2)
O(6)	0.6040(3)	0.3551(2)	−0.0834(2)
O(7)	0.8264(2)	0.3627(2)	0.0554(2)
O(8)	0.6476(3)	0.1964(2)	0.0471(2)
O(9)	0.3233(3)	0.4074(2)	0.0310(2)
N(1)	0.2041(3)	0.0615(2)	0.0081(2)
N(2)	0.0506(2)	−0.0286(2)	−0.1445(2)
C(1)	0.3278(3)	0.0803(2)	−0.0631(2)
C(2)	0.3169(3)	0.0470(2)	−0.1769(2)
C(3)	0.1760(3)	−0.0087(2)	−0.2137(2)
C(4)	0.0701(3)	0.0088(2)	−0.0375(2)

Table 4 Selected interatomic distances (Å) and bond angles (°) for complex **1** with e.s.d.s in parentheses[a]

Nickel environment

Ni(1)–O(1)	2.045(3)	Ni(1)–O(2)	2.063(3)
Ni(1)–O(3)	2.044(3)	Ni(1)–O(4)	2.047(3)
Ni(1)–N(1)	2.092(3)	Ni(1)–N(2a)	2.097(3)
O(1)–Ni(1)–O(2)	92.3(1)	O(1)–Ni(1)–N(2a)	171.0(1)
O(1)–Ni(1)–N(1)	91.8(1)	O(1)–Ni(1)–O(3)	89.6(1)
O(1)–Ni(1)–O(4)	89.6(1)	O(2)–Ni(1)–N(2a)	96.7(1)
O(2)–Ni(1)–N(1)	175.2(1)	O(2)–Ni(1)–O(3)	88.2(1)
O(2)–Ni(1)–O(4)	85.8(1)	N(1)–Ni(1)–N(2a)	79.2(1)
O(3)–Ni(1)–N(2a)	91.2(1)	O(4)–Ni(1)–N(2a)	90.5(1)
O(3)–Ni(1)–N(1)	94.5(1)	O(4)–Ni(1)–N(1)	91.6(1)
O(3)–Ni(1)–O(4)	173.9(1)		

Hydrogen bonds[b]

A	D	H	A···D	A···H–D
O(8b)	O(1)	H(1w)	2.75(1)	159(2)
O(6)	O(1)	H(2w)	2.79(1)	166(3)
O(5)	O(2)	H(4w)	2.76(1)	175(3)
O(8)	O(3)	H(5w)	2.81(1)	167(3)
O(5c)	O(3)	H(6w)	2.76(1)	165(3)

[a] Symmetry codes: (a) $-x, -y, -z$; (b) $\frac{1}{2} - x, \frac{1}{2} + y, \frac{1}{2} - z$; (c) $\frac{1}{2} + x, \frac{1}{2} - y, \frac{1}{2} + z$. [b] A = Acceptor, D = donor.

(see the end of Tables 4 and 5). As shown in Fig. 2, a crystallization water molecule in **2** links two co-ordinated water molecules from two dinuclear entities through hydrogen bonding, the resulting intermolecular Ni(1)···Ni(1d) separation being 6.760(1) Å.

The geometry around the nickel atoms in both compounds is almost identical: the environment of the metal ion is slightly distorted from that of a regular octahedron with two nitrogen atoms from bipym and four oxygen atoms from water molecules. The bipym ligand joins two adjacent co-ordination polyhedra with its nitrogen atoms occupying two *cis* positions in both polyhedra. The four nickel to oxygen bonds average 2.050(3) (**1**) and 2.056(2) Å (**2**), and the mean values for the nickel to nitrogen bonds are 2.094(3) (**1**) and 2.115(2) Å (**2**). There is slight evidence of distortion along the O(2)–Ni(1)–N(1) axis in **1** as the nickel–oxygen bond is lengthened to 2.063(3) Å from 2.045 Å for the other nickel–oxygen bonds. The occurrence of three different nickel–oxygen distances in **2** [2.082(2), 2.067(2) and 2.039(2)–2.037(2) Å] makes more evident this distortion. The average Ni^{II}–N(bipym) distance is shorter than those reported for bipym-bridged iron(II) (2.32 Å)[5e] and cobalt(II) (2.16 Å)[5c] but greater than that of copper(II) (2.06 Å)[5f,8] in agreement with the decreasing ionic radii in the series

Table 5 Selected interatomic distances (Å) and bond angles (°) for complex **2** with e.s.d.s in parentheses[a]

Nickel environment

Ni(1)–O(1)	2.082(2)	Ni(1)–O(2)	2.039(2)
Ni(1)–O(3)	2.037(2)	Ni(1)–O(4)	2.067(2)
Ni(1)–N(1)	2.125(2)	Ni(1)–N(2a)	2.105(2)
O(1)–Ni(1)–O(2)	91.9(1)	O(1)–Ni(1)–N(2a)	176.1(1)
O(1)–Ni(1)–N(1)	97.6(1)	O(1)–Ni(1)–O(3)	85.3(1)
O(1)–Ni(1)–O(4)	89.9(1)	O(2)–Ni(1)–N(2a)	92.0(1)
O(2)–Ni(1)–N(1)	170.3(1)	O(2)–Ni(1)–O(3)	87.2(1)
O(2)–Ni(1)–O(4)	89.5(1)	N(1)–Ni(1)–N(2a)	78.5(1)
O(3)–Ni(1)–N(2a)	94.9(1)	O(4)–Ni(1)–N(2a)	90.2(1)
O(3)–Ni(1)–N(1)	91.6(1)	O(4)–Ni(1)–N(1)	92.5(1)
O(3)–Ni(1)–O(4)	174.0(1)		

Hydrogen bonds[b]

A	D	H	A···D	A···H–D
O(6)	O(1)	H(1w)	2.84(1)	173(3)
O(8b)	O(1)	H(2w)	2.74(1)	167(3)
O(5c)	O(2)	H(3w)	2.79(1)	162(2)
O(7d)	O(3)	H(5w)	2.70(1)	174(2)
O(5e)	O(4)	H(7w)	2.72(1)	169(3)
O(7f)	O(4)	H(8w)	2.76(1)	174(3)
O(6b)	O(9)	H(9w)	2.74(1)	171(3)

[a] Symmetry codes: (a) $-x, -y, -z$; (b) $1-x, 1-y, -z$; (c) $-x, -\frac{1}{2}+y, \frac{1}{2}-z$; (d) $-x, 1-y, -z$; (e) $x, -1+y, z$; (f) $x, \frac{1}{2}-y, \frac{1}{2}+z$. [b] A = Acceptor, D = donor.

$Fe^{II} > Co^{II} > Ni^{II} > Cu^{II}$. Significant deviations from idealized orthogonal geometry are found at the nickel atom in the five-membered Ni(1)N(1)C(4)C(4a)N(2a) chelate ring [79.2(1) and 78.5(1)° for N(1)–Ni(1)–N(2a) in **1** and **2**, respectively] as expected due to the short bite distance of the free bipym (2.63 Å).[14]

The pyrimidyl rings of bipym are planar as expected with deviations from the mean planes not greater than 0.006 Å in complex **1** and 0.012 Å in **2**. The bipym ligand as a whole is also planar. The carbon–carbon and –nitrogen intra-ring bonds compare favourably with the parent values observed in uncoordinated,[14] chelating,[5h,6e–h,8,9] and bis(chelating)[5b,c,e–h,8,9] bipym. The carbon–carbon inter-ring bond length (1.47 Å) is somewhat shorter than the classical value of 1.54 Å for the C–C bond distance. The nickel atom is 0.070 (**1**) and 0.034 Å (**2**) out of the bipym plane. Atoms O(1), O(2), N(1) and N(1a) fall in a plane (maximum deviations of 0.024 and 0.020 Å for **1** and **2**, respectively). With respect to this plane, the nickel atom is pulled toward O(4) by 0.024 Å in **1** and 0.016 Å in **2**. The dihedral angle between the bipym and O(1)O(2)N(1)N(1a) plane is 3.6° for **1** and 1.8° for **2**. The nickel–nickel separation through bipym, Ni(1)···Ni(1a), is 5.569(1) Å in **1** and 5.660(1) Å in **2**, whereas the shortest intermolecular metal–metal distance is somewhat larger [7.439(1) and 6.686(1) Å in **1** and **2**, respectively].

The nitrate and sulfate anions have their expected trigonal and tetrahedral geometries, respectively. The nitrate group is planar with no deviations greater than 0.011(3) Å from the mean plane of the four atoms. The nitrogen–oxygen bond lengths and the intra-anion bond angles average 1.234 Å and 120°, respectively. However, the values of two of the bond angles deviate significantly from the ideal value [114.2(4) and 125.5(5)° for O(8)–N(4)–O(9) and O(9)–N(4)–O(10), respectively]. The average values of the sulfur–oxygen bond distance and intra-ion bond angle for the sulfate group are 1.471 Å and 109.5°.

Electronic and Infrared Spectra.—The absorption spectra of complexes **1** and **2** are typical of octahedral nickel(II) complexes,[15] exhibiting the three-spin allowed transitions from $^3A_{2g}$ to $^3T_{2g}$, $^3T_{1g}$ and $^3T_{1g}$ (P) at 9300 (ν_1), 15 750 (ν_2) and 26 600 (ν_3) cm^{-1} (**1**) and at 9220 (ν_1), 15 670 (ν_2) and 25 980 (ν_3) cm^{-1} (**2**), as expected for a d^8 configuration in a near-octahedral ligand field. The values of $10Dq$ for **1** (9300 cm^{-1}) and **2** (9220 cm^{-1}) are very similar due to the occurrence of the same chromophore with only slight differences in the bond lengths and angles at the metal ion. For the octahedral case, by calculation in the strong-field coupling scheme with a d^8 configuration, the Racah parameter B is found to be 914 (**1**) and 898 cm^{-1} (**2**) leading to a nepheulauxetic ratio of 0.866 (**1**) and 0.850 (**2**) [considering that $15B$ has a value of 15 840 cm^{-1} for the gaseous ion (^3P) for Ni^{2+}]. With the g values of **1** and **2**, obtained from the best fit of the magnetic susceptibility measurements (see below), and through the equation $g = 2 - 8\lambda/10Dq$, an average value of -122 cm^{-1} is calculated for the spin–orbit coupling constant. A shoulder is observed on the middle band at 13 700 (**1**) and 13 600 cm^{-1} (**2**). This splitting is due to spin–orbit coupling which mixes the $^3T_{1g}$ (F) and ^1E_g states, which are very close in energy for $10Dq$ values of *ca.* 9000 cm^{-1}.[16]

The most important aspect of the IR spectra of complexes **1** and **2** concerns the bands of bipym. The occurrence of a very asymmetric doublet at 1585s and 1563w cm^{-1} (ring-stretching modes of bipym) is proof of the bridging role of this organic ligand as observed in bipym-bridged copper(II) complexes.[5b,f,9] It was pointed out that these two stretching modes of bipym appear as two sharp features of nearly equal intensity at the above-mentioned wavenumbers when it acts as an end-cap ligand.[6f]. Another ring-stretching mode which appears as a strong feature at 1400 cm^{-1} for unco-ordinated bipym is also observed at 1420 cm^{-1} for compounds **1** and **2**.

Magnetic Properties.—The thermal dependence of the molar magnetic susceptibility χ_M of complexes **1** and **2** is characteristic of an antiferromagnetic interaction between the two single-ion triplet states: the value of χ_M at room temperature is in the range expected for two $S = 1$ states [$\mu_{eff} = 4.14$ (**1**) and 4.10 (**2**)], increases as the temperature is lowered until a maximum is reached ($T_{max} = 20.5$ K for **1** and 18 K for **2**) and finally exhibits a rapid decrease (see Figs. 3 and 4).

The ground state of a nickel(II) in an octahedral environment is orbitally non-degenerate and as such it is possible to represent the intradimer magnetic interaction (J) with the isotropic spin Hamiltonian $\hat{H} = -J\hat{S}_A\cdot\hat{S}_B$. The molar magnetic susceptibility for a nickel(II) dimer ($S_A = S_B = 1$) is thus given by equation (1) where N, β, k, g and T have their usual meanings and it is

$$\chi_M = \frac{2N\beta^2g^2}{kT}\left[\frac{\exp(J/kT) + 5\exp(3J/kT)}{1 + 3\exp(J/kT) + 5\exp(3J/kT)}\right] \quad (1)$$

assumed that $g_x = g_y = g_z = g$. Although nickel(II) in axial symmetry can have a large zero-field splitting, D, the magnetic behaviour of nickel(II) dimers closely follows equation (1) when a relatively strong antiferromagnetic interaction is operative. If the antiferromanetic coupling is weak or the coupling is ferromagnetic, the effect of D can be relevant to describe the magnetic behaviour at low temperatures.

Ginsberg *et al.*[17a] and Journaux[17b] have considered the effect of D on the magnetic susceptibility of nickel(II) dimers [$\hat{H} = -J\hat{S}_A\cdot\hat{S}_B - D(\hat{S}_{zA}^2 + \hat{S}_{zB}^2)$]. In this case, the molar magnetic susceptibility for a nickel(II) dimer is given by expression (2)

$$\chi_M = \frac{2N\beta^2g^2}{3\alpha}\left(\frac{F_1}{kT} + \frac{2F_2}{D} + \frac{6a^2F_3}{3J-\Delta} + \frac{6b^2F_4}{3J+\Delta}\right) \quad (2)$$

where $F_1 = 1 + \exp(2x) + 4\exp(2x+y)$, $F_2 = -1 + 2\exp(2x+y) + \exp(y) - 2\exp(2x)$, $F_3 = \exp(2x) - \exp(\frac{x}{2}+z)$, $F_4 = \exp(2x) - \exp(\frac{x}{2}-z)$, $\alpha = 2 + \exp(y) + \exp(\frac{x}{2}-z) + \exp(\frac{x}{2}+z) + 2\exp(2x) + 2\exp(2x+y)$, $x = J/kT$, $y = D/kT$, $z = \Delta/kT$, $\Delta = [(3J+D)^2 - 8JD]^{\frac{1}{2}}$, $a = (9J - D + 3\Delta)/[(9J - D + 3\Delta)^2 + 8D^2]^{\frac{1}{2}}$ and $b = 2\sqrt{2}D/[(9J - D +$

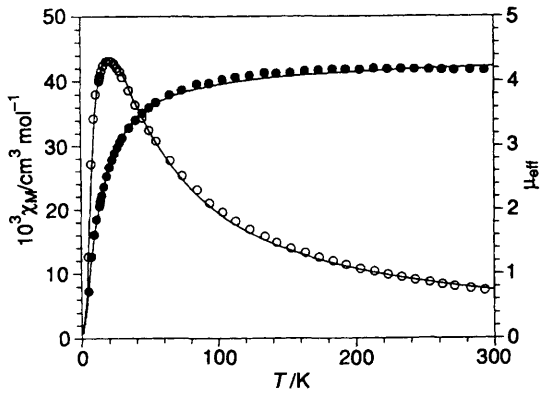

Fig. 3 Thermal dependence of the molar magnetic susceptibility (○) and μ_{eff} (●) for complex **1**. The solid line corresponds to the best theoretical fit (see text)

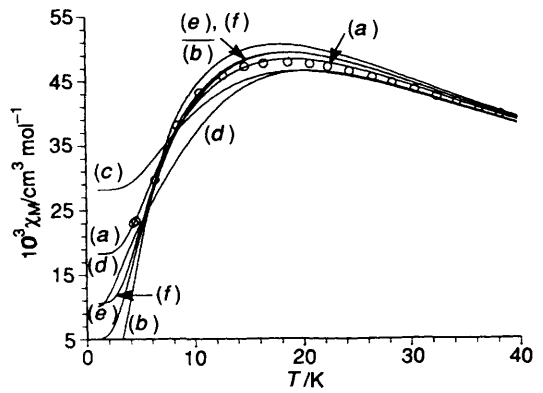

Fig. 4 Thermal dependence of the molar magnetic susceptibility (○) for complex **2**. Curve (*a*) corresponds to the best theoretical fit with $J = -12$ cm^{-1}, $g = 2.10$ and $D = -14$ cm^{-1}. The remaining curves illustrate the influence of D on the magnetic curve [$D = 0$ (*b*), 20 (*c*), -20 (*d*), 10 (*e*) and -10 cm^{-1} (*f*)] for the same J and g values as for (*a*)

$3\Delta)^2 + 8D^2]^{\frac{1}{2}}$. Least-squares analysis of all data for complexes **1** and **2** using equation (2) led to $J = -14$ cm^{-1}, $g = 2.11$ and $D = -1.7$ cm^{-1} (**1**) and $J = -12$ cm^{-1}, $g = 2.10$ and $D = -14$ cm^{-1} (**2**). The agreement factor R defined as $\Sigma_i[(\chi_M)_{obs}(i) - (\chi_M)_{calc}(i)]^2/\Sigma_i[(\chi_M)_{obs}(i)]^2$ is equal to 3.2×10^{-4} for **1** and 1.9×10^{-4} for **2**.

Ginsberg has also treated interdimer interactions in the context of the molecular field approximation ($-z'J'\hat{S}_z\langle\hat{S}_z\rangle$, where z' is the dimer lattice co-ordination number, J' is the effective interdimer coupling and S_z is the operator for the z component of the total dimer spin). When we take into account this interdimer interaction, very small values of $z'J'$ were found for complexes **1** and **2** and they do not improve the quality of the fit. The large interdimer separation in both compounds (>6.6 Å) accounts for this weak intramolecular exchange interaction.

A good fit is also obtained for the experimental data of complex **1** through equation (1), whereas it is not good for compound **2**, revealing that it is necessary to take into account the zero-field splitting effects in this latter case. In order to analyse the influence of D on the magnetic susceptibility of **2**, we have kept constant its J and g values and varied D as shown in Fig. 4. The effect of D on χ_M only consists of displacing the χ_M curve *versus* T along the susceptibility axis, the position of the maximum being essentially unchanged. Since the temperature of the maximum of χ_M determines the value of J, it can be concluded that the value of D has no influence on the J value. Analogous considerations can be made regarding the $z'J'$ value.

The difficulty in obtaining accurate D values from powder susceptibility data merits comment. This is apparent from an inspection of Fig. 4. The value of D can be seen to be significant only in the low-temperature region and is of minor importance at temperatures above the peak; D is the only parameter that influences the susceptibility curve to any extent in the low-temperature region. Moreover, it is not possible to determine the sign of D. A similar fit was found for positive values of D [3.1 (**1**) and 17 cm^{-1} (**2**)]. Values of D of 3–10 cm^{-1} for dinuclear nickel(II) complexes[18] and about 20 cm^{-1} for nickel(II) chains[19] have been reported. The greater $|D|$ value of **2** with respect to that of **1** cannot be ascribed to the somewhat greater distortion of the NiN_2O_4 chromophore in **2**. Our feeling is that this parameter has been overestimated in the fit. However, the experimental susceptibilities of **2** cannot be fitted for a $|D|$ value similar to that of **1** except if the intermolecular interactions $z'J'$ attain a value of *ca.* -4 cm^{-1}. This value is clearly unreal in the light of the structure of **2**. If the presence of paramagnetic impurities is taken into account the fit is not improved. Therefore, our conclusion is that the $|D|$ value of **2** must be much smaller than 14 cm^{-1} and its influence is illustrated by Fig. 4.

As the symmetry of each nickel(II) in complexes **1** and **2** is roughly C_{2v} we have investigated the possible influence of the rhombic distortion parameter (E) on the magnetic susceptibility. When this parameter [$E(\hat{S}_{xA}^2 + \hat{S}_{xB}^2) - (\hat{S}_{yA}^2 + \hat{S}_{yB}^2)$] is introduced in the above-mentioned Hamiltonian, the energy matrix becomes very complicated and no analytical expression for χ_M can be obtained. In this case only a numerical solution is available.[17b] Given that the values of E are in general very small (≈ 1 cm^{-1}) we have analysed its influence on χ_M once the values of the other adjustable parameters (J, g and D) were known. We found that the fit was not significantly improved and that the J, g and D values were not affected.

No polycrystalline powder ESR spectrum could be detected for complexes **1** and **2** because of the large zero-field splitting of the nickel(II) ions.

The values of J for complexes **1** and **2** are very close to those previously reported for other bipym-bridged nickel(II) complexes of formula $[Ni_2(hfacac)_4(bipym)]$, $[Ni_2(tfacac)_4(bipym)]$ and $[Ni_2(tfpacac)_4(bipym)]$ (J ranging from -13 to -11.2 cm^{-1})[5c] where tfacac and tfpacac are trifluoroacetylacetonate and its phenyl derivative, respectively. No structure was reported for these complexes because the unavailability of single crystals. The magnitude of the exchange coupling can be classified as intermediate taking into account that the spin coupling occurs between nickel(II) ions separated by distances greater than 5.5 Å. This efficiency of bis(bidentate) bipym to transmit electronic effects at such distances was analysed in a previous contribution,[5f] and it is mainly due to the strong overlap between the $d_{x^2-y^2}$ magnetic orbitals centred on the metal ions [x and y axis being roughly defined by the Ni–N(bipym) bonds] through the symmetry-adapted highest-occupied molecular orbital (HOMO) of the bipyrimidine bridge. The fact that the Ni(bipym)Ni fragment is practically planar favours the overlapping and increases the magnitude of the coupling.

Finally, concerning the spin coupling in dinuclear nickel(II) complexes, we would compare the relative efficiency of bis-chelating) C_2XYZW-type ligands such as bipym (X = Y = Z = W = N), oxalate (X = Y = Z = W = O) and oxamidate (X = W = N, Y = Z = O). The observed J values for the

complexes $[Ni_2(cyclam)_2(ox)][NO_3]_2$[20] (cyclam = 1,4,8,11-tetraazacyclotetradecane, ox = oxalate) and $[Ni_2\{(O_2CCH_2NCO)_2\}(H_2O)_6]\cdot 4H_2O$[21] are -39 and -25 cm^{-1}, respectively. The trend exhibited by the J values, $|J|_{oxalate} > |J|_{oxamidate} > |J|_{bipym}$, is at first sight somewhat surprising. Extended-Hückel calculations have shown that the less electronegative the atoms of the bridge the higher is the delocalization of the spin density on them, and consequently the greater is the antiferromagnetic

coupling[22-24] everything being equal. The expected trend in this context would be just the opposite, $|J|_{oxalate} < |J|_{oxamidate} < |J|_{bipym}$. Three factors allow us to account for this unexpected trend: (*i*) the stabilization by resonance of the HOMO of bipym, (*ii*) the difference in the planarity of the Ni(bridge)Ni fragment and (*iii*) the intramolecular metal–metal separation. The resonance which is operative in bipym stabilizes its symmetry-adapted HOMO which overlaps with the in-phase and out-of-phase combinations of the $d_{x^2-y^2}$ magnetic orbitals of nickel(II), and reduces the spin density at the bridging atoms. Moreover, the intramolecular nickel–nickel separation in the bipym complexes is 5.569(1) in **1** and 5.660(1) Å in **2**, values which are greater than those of the oxamidato (5.368 Å) and oxalato (5.395 Å) compounds. These two factors reduce the efficiency of the bipym to transmit electronic effects with respect to oxalate and oxamidate. As far as the last point is concerned, the Ni(bipym)Ni and Ni(ox)Ni entities are practically planar, whereas the metal ion is 0.228 Å out of the Ni(oxamidate)Ni mean plane. Such a significant distortion accounts for the lowering of the efficiency of oxamidate with respect to oxalate.

Acknowledgements

Financial support from the Dirección General de Investigación Científica y Técnica (DGICYT) (Spain) through Project PB91-0807-C02-01 and from the Italian Ministero dell' Università e della Ricerca Scientifica e Tecnologica are gratefully acknowledged. Thanks are also due to the Servicio de Espectroscopía de la Universitat de València for instrumental facilities.

References

1 A. Tuerstein, B. A. Feit and G. Navon, *J. Inorg. Nucl. Chem.*, 1974, **36**, 1055.
2 M. Hunziker and A. Ludi, *J. Am. Chem. Soc.*, 1977, **99**, 7370; E. V. Dose and L. J. Wilson, *Inorg. Chem.*, 1978, **17**, 2660; D. P. Dillema, R. W. Callahan and K. B. Mack, *Inorg. Chem.*, 1982, **21**, 2589; R. R. Ruminski and J. D. Petersen, *Inorg. Chem.*, 1982, **21**, 3706.
3 R. H. Petty and L. J. Wilson, *J. Chem. Soc., Chem. Commun.*, 1978, 483; R. H. Petty, B. R. Welch, L. J. Wilson, L. A. Bottomley and K. M. Kadish, *J. Am. Chem. Soc.*, 1980, **102**, 611; G. A. Brewer and E. Sinn, *Inorg. Chem.*, 1984, **23**, 2532.
4 A. Overton and J. A. Connor, *Polyhedron*, 1982, **1**, 53; W. Kaim, *Inorg. Chem.*, 1984, **23**, 3365; W. Kaim and S. Kohlmann, *Inorg. Chem.*, 1986, **25**, 3306; S. Lanza and E. Rotondo, *Inorg. Chim. Acta*, 1988, **146**, 205; G. Matsubayashi, Y. Yamaguchi and T. Tanaka, *J. Chem. Soc., Dalton Trans.*, 1988, 2215.
5 (*a*) S. Lanza, *Inorg. Chim. Acta*, 1983, **75**, 131; (*b*) G. De Munno and G. Bruno, *Acta Crystallogr., Sect. C*, 1984, **40**, 2030; (*c*) G. Brewer and E. Sinn, *Inorg. Chem.*, 1985, **24**, 4580; (*d*) K. J. Brewer, W. R. Murphy and J. D. Petersen, *Inorg. Chem.*, 1987, **26**, 3376; (*e*) A. Real, J. Zarembowitch, O. Kahn and X. Solans, *Inorg. Chem.*, 1987, **26**, 2939; (*f*) M. Julve, G. De Munno, G. Bruno and M. Verdaguer, *Inorg. Chem.*, 1988, **27**, 3160; (*g*) L. W. Morgan, K. V. Goodwin, W. T. Pennington and J. D. Petersen, *Inorg. Chem.*, 1992, **31**, 1103; (*h*) G. De Munno, G. Bruno, F. Nicolo', M. Julve and J. A. Real, *Acta Crystallogr.*, in the press.
6 (*a*) R. R. Ruminski, K. D. Van Tassel and J. D. Petersen, *Inorg. Chem.*, 1984, **23**, 4380; (*b*) R. R. Ruminski and J. D. Petersen, *Inorg. Chim. Acta*, 1984, **88**, 63; (*c*) R. R. Ruminski and J. D. Petersen, *Inorg. Chim. Acta*, 1985, **97**, 129; (*d*) R. R. Ruminski, *Inorg. Chim. Acta*, 1985, **103**, 159; (*e*) G. De Munno, G. Bruno, M. Julve and M. Romeo, *Acta Crystallogr., Sect. C*, 1990, **46**, 1828; (*f*) I. Castro, M. Julve, G. De Munno, G. Bruno, J. A. Real, F. Lloret and J. Faus, *J. Chem. Soc., Dalton Trans.*, 1992, 1739; (*g*) L. W. Morgan, W. T. Pennington, J. D. Petersen and R. R. Ruminski, *Acta Crystallogr., Sect. C*, 1992, **48**, 163; (*h*) G. De Munno, F. Nicolo' and M. Julve, *Acta Crystallogr., Sect. C*, in the press.
7 W. Kaim and S. Kohlmann, *Inorg. Chem.*, 1987, **26**, 68 and refs. therein.
8 G. De Munno, M. Julve, M. Verdaguer and G. Bruno, *Inorg. Chem.*, in the press.
9 M. Julve, M. Verdaguer, G. De Munno, J. A. Real and G. Bruno, *Inorg. Chem.*, in the press.
10 A. C. T. North, D. C. Phillips and F. S. Mathews, *Acta Crystallogr., Sect. A*, 1968, **24**, 351.
11 SHELXTL PLUS, Version 3.4, Siemens Analytical X-ray Instruments, Madison, WI, 1989.
12 *International Tables for X-Ray Crystallography*, Kynoch Press, Birmingham, 1974, vol. 4, pp. 72–99.
13 M. Nardelli, *Comput. Chem.*, 1983, **7**, 95.
14 L. Fernholt, C. Rømming and S. Samdal, *Acta Chem. Scand., Ser. A*, 1981, **35**, 707.
15 F. A. Cotton and G. Wilkinson, *Advanced Inorganic Chemistry*, 4th edn., Wiley, New York, 1980.
16 See ref. 15, p. 787.
17 (*a*) A. P. Ginsberg, R. L. Martin, R. W. Brookes and R. C. Sherwood, *Inorg. Chem.*, 1972, **11**, 2884; (*b*) Y. Journaux, Thèse de 3e cycle, Orsay, 1978.
18 A. Vermaas, W. L. Groeneveld and J. Reedjik, *Z. Naturforsch., Teil A*, 1977, **32**, 632.
19 H. T. Witteveen, W. L. C. Rutten and J. Reedijk, *J. Inorg. Nucl. Chem.*, 1975, **37**, 913.
20 L. P. Battaglia, A. Bianchi, A. Bonamartini-Corradi, E. García-España, M. Micheloni and M. Julve, *Inorg. Chem.*, 1988, **27**, 4174.
21 F. Lloret, J. Sletten, R. Ruiz, M. Julve and M. Verdaguer, *Inorg. Chem.*, 1992, **31**, 778.
22 M. Verdaguer, O. Kahn, M. Julve and A. Gleizes, *Nouv. J. Chim.*, 1985, **9**, 325.
23 R. Vicente, J. Ribas, S. Alvarez, A. Segui, X. Solans and M. Verdaguer, *Inorg. Chem.*, 1987, **26**, 4004.
24 S. Alvarez, M. Julve and M. Verdaguer, *Inorg. Chem.*, 1990, **29**, 4500.

Received 7*th October* 1992; *Paper* 2/05391H